The SLEGS beamline of SSRF*

Liu Long-Xiang,[1] Wang Hong-Wei,[1,†] Fan Gong-Tao,[1,‡] Xu Hang-Hua,[1] Zhang Yue,[1] Hao Zi-Rui,[1] and Li Ai-Guo[1,§]

[1]*Shanghai Advanced Research Institute,Chinese Academy of Sciences (CAS),Shanghai 201210, China*

The Shanghai Laser Electron Gamma Source(SLEGS, located in BL03SSID) beamline at Shanghai Sychrotron Radiation Facility(SSRF) is a Laser Compton Scattering(LCS) gamma source, for investigating nuclear structure, which is demanded extensively in the fields of nuclear astrophysics, nuclear cluster structure, polarization physics, nuclear energy and so on. The beamline is based on the inverse Compton scattering of 10640 nm photons on 3.5 GeV electrons and a gamma source with variable energy by changing the scattering angle from 20 degree to 160 degree. γ-rays of 0.25-21.1 MeV can be extracted by the scheme consisting of interaction chamber,coarse collimator,fine collimator and attenuator. The maximum photon flux for 180 degree about 10^7 photons/s at the target at 21.7 MeV, with a beam size of 3 mm diameter. The beamline is equipped with four types of spectrometers for experiments in (γ,γ'), (γ,n) and (γ,p\α). At present, Nuclear Resonance Fluorescence (NRF) spectrometer, Flat Efficiency neutron Detector (FED) spectrometer, Neutron Time-Of-Flight (TOF) spectrometer and Light Charged Particle (LCP) spectrometer methods have been developed.

Keywords: Shanghai Sychrotron Radiation Facility, SLEGS, nuclear astrophysics, nuclear structure

I. INTRODUCTION

In the past few decades, γ-photon beams are steadily developing and have optimized beam properties, which can be used for research and applications. The past and future development of photon sources can generally be divided into five generations [1]. The first generation of photon sources utilized various artificially induced γ-radioactivity of various excited nuclei, such as ^{137}Cs,^{60}Co,^{27}Al(p,γ)^{28}Si,and so on. Such sources are mainly used for detector calibration and irradiation experiments. The energy of this type of photon source is fixed.

The second generation MeV range photon source is generated by bremsstrahlung or positron annihilation. A very simple way to produce a strong photon bath with a continuous energy distribution is electron bremsstrahlung. Nowadays, the energy spectra of bremsstrahlung photons are usually calculated using different Monte Carlo simulation codes [2–4]. The main difficulty is to extract bremsstrahlung flux close to the end energy of the spectrum. The energy of the electron beam and its fluctuations play a decisive role. Therefore, careful monitoring of the energy of the electron beam is mandatory for many experiments. The bremsstrahlung γ-photon source adjusts the maximum gamma energy by adjusting the energy of the incident electron. It either provides broad-band γ-photon or low-intensity beams with some energy resolution through the method of electron energy-tagging. These sources have greatly expanded the field of photonuclear science in the past.

The Darmstadt High Intensity Photon Device (DHIPS) uses a continuous wave electron beam to generate photon beams, typically with maximum energies up to 10 MeV and currents up to 60 μA [5]. The γELBE facilities use superconducting continuous electron linear accelerators with a current up to 1 mA and a maximum energy of 13 MeV to produce a bremsstrahlung beam [3]. At the Flerov Laboratory of Nuclear Reactions of the Joint Institute for Nuclear Research in Dubna, Russia, the Bremsstrahlung facility of the MT-25 microtron delivers presently an electron beam in the energy range from 10 to 25 MeV with an average electron current of up to 20 μA [6]. The recently installed S band accelerator PRISM at the Lawrence Livermore Laboratory in Livermore, CA, USA, operates with an electron energy between 15 and 25 MeV and currents up to 30 μA [7]. At the High Voltage Research Laboratory (HVRL) of the Massachusetts Institute of Technology (MIT), an electron accelerator with energy up to about 3.5 MeV and currents in the 100 μA range can be used for Nuclear Resonance Fluorescence experiments [8] . The NSC KIPT in Kharkov, Ukraine operates an S-band e-linac (LUE-40) which can be used for photoactivation experiments in the energy range between about 35 and 95 MeV with the typical average electron current amounts to 6 μA [9]. At Idaho State University, USA, four e-linacs with maximum electron energies up to 40 MeV is utilized to generate the bremsstrahlung beam [10]. The maximum electron current is between 85 and 240 μA.

Due to the provision of information about the energy of the generated bremsstrahlung photons by the technique of tagged photons, the photon nuclear reaction caused by bremsstrahlung photons can determine the energy-resolved reaction cross sections. The photon tagger NEPTUN at the S-DALINAC at the TU Darmstadt covers photon energies from below the particle emitting threshold to above the IVGDR region for photon scattering and total photoabsorption experiments which determine the complete dipole strength [11].

At present, the most common sources are the third generation which are the scattering of electrons in synchrotrons or storage rings using the principle of laser Compton backscattering. The High Intensity γ-Ray Source (HIγS) facility has been the most productive example in the past [12, 13]. It is operated by the Triangle Universities Nuclear Laboratory at the Duke University,and can provide nearly mono-energetic polarized gamma ray beams with an energy range of 1 to 100 MeV, with a maximum total intensity of approximately

* Supported by the Shanghai Light Source Line Station Project
† Corresponding author, wanghw@sari.ac.cn
‡ Corresponding author, fangt@sari.ac.cn
§ Corresponding author, liag@sari.ac.cn

3×10^{10} photons/s near 10 MeV. The maximum gamma ray energy of the laser Compton scattering gamma-ray source in the UVSOR-III storage ring is 5403 keV, and the total available flux is 1×10^7 photons/s, sufficient for basic research on non-destructive three-dimensional isotopes [14]

Compared to existing facilities, some new LCB facilities with further improved parameters have been announced to be put into operation in the coming years. As an example, the Variable Energy Gamma-Ray System (VEGA) at the international research center Extreme Light Infrastructure-Nuclear Physicas (ELI-NP) in Romania, will be briefly introduced. By selecting one of the two interacting lasers and adjusting the electron energy in the storage ring accordingly, the energy range of the generated photon beam can continuously vary between 1 and 20 MeV. For Compton backscattered laser photons, a small electron beam emittance produces a small bandwidth of approximately or even less than 0.5%. The total photon flux will be greater than 10^{11} photons/s, and the time-averaged spectral intensity of collimation at the maximum position will be greater than 5×10^3 photons per second and eV [1].

There are two main ways to increase beam intensities in the fourth generation gamma source. One method to achieve higher intensity is based on the multi-bunch multi-pulse concept proposed by Chris Barty and coworkers, where a laser beam collides with an electron microbeam with small temporal spacing [1]. Another method is a superconducting radio-frequency (SRF) and superconducting multi-turn energy-recovery linac (ERL). In fact, the international ERL community has recently published a corresponding superconducting multi-turn energy-recovery linac conceptional design report [15]. An SRF-ERL would generate a continuous electron beam with extremely low emittance and very high current, which can generate LCB photon beams with further reduced bandwidth (down to the per mille range) and higher intensity.

The relatively small cross-section of Compton scattering within the barn range defines a limitation on the maximum photon flux that can be obtained from laser Compton backscattering devices. A few years ago, a principle was proposed to overcome this limitation, which is currently known as the fifth generation gamma source of the "Gamma Factory at CERN" [16, 17]. This idea is to use a partially stripped ultra-relativistic ion beam, which undergo atomic transitions after resonant absorption of laser photons. Because the energy of the emitted photons is boosted by one factor, up to four times the square of the Lorentz factor of the particle beam, this means that the energy range of the tunable photon beam at LHC is approximately 1-400 MeV. Compared to the laser Compton scattering on the point-like electron, the cross-section of laser photon absorption is much larger (within the Gbarn range), thus achieving unprecedented γ beam intensity. Many possible applications have been discussed, such as referring to references [18, 19].

The SLEGS, belonging to the third-generation gamma source, is one of the Phase II beamline at Shanghai Synchrotron Radiation Facility (SSRF), a third generation light source with a 3.5 GeV storage ring running 200 mA electron beam current in the top-up injection mode [20–28].

Photon-induced nuclear reactions with energies higher than the particle binding energy are capable of obtaining information on the electromagnetic decay strength of Giant Dipole Resonance (GDR) with multipole selectivity and the coupling of GDR to low-frequency collective modes [29–32]. The Pygmy Dipole Resonance(PDR) can be used to understanding the entire E1 response of nuclei and the nuclear symmetry energy in the Equation Of State (EOS) for nuclear matter [33, 34]. Magnetic dipole resonance(MDR) above neutron threshold with PDR around neutron threshold constitute extra strengths of the low energy γ-ray strength function [35, 36]. Dedicated for GDR,PDR and MDR measurement, the construction of SLEGS was completed in December 2021 and has been opened to users since September 2023 [37]. After experts of SSRF review, the first users from domestic universities and research institutes will successively carry out experimental research on photonuclear reactions and photon activation analysis(PAA). In this paper, we present a review on the facilities and experimental methods of the SLEGS beamline.

II. THE BEAMLINE

A. The gamma source

The main SLEGS beamline components that generate gamma rays include the interaction chamber, the multi-function chamber, and the CO2 laser [38]. Laser generates back-scattered gamma energy of 21.7 MeV through the multi-function chamber. Laser can produce gamma rays with a Compton edge energy range of 0.66-21.1 MeV from 20 degree to 160 degree through the interaction chamber in the slant scattering mode. The energy of gamma is continuously adjustable by changing the scattering angle between laser and electron.

The frequency of the SLEGS gamma source is determined by the frequency of the laser, which is 1kHz. Therefore, the time distribution of laser gamma within a millisecond time cycle can be obtained by utilizing the time of gamma events, as shown in Fig. 1 (a). It is consistent with the distribution of laser within a clock cycle. Laser gamma events and background gamma events can be distinguished based on time distribution. By using this method, the background events in laser gamma can be deducted to obtain the energy spectrum distribution of laser gamma, as shown by the red line in Fig. 1 (b). Using the method can reduce the measurement time of the experiment and improve the utilization of beam time. All spectrometers on the experimental station can also use this method to deduct background.

To successfully conduct experiments on the station, it is necessary to accurately obtain the gamma spectrum distribution of each laser angle, so measuring the gamma spectrum is very important. Monoenergetic gamma sources of 6.13 MeV, 9.17 MeV, 10.76 MeV, and 17.6 MeV were obtained by bombarding ^{19}F, ^{13}C, ^{27}Al, and ^{7}Li targets with proton sources from the Chinese Institute of Atomic Energy to calibrate the

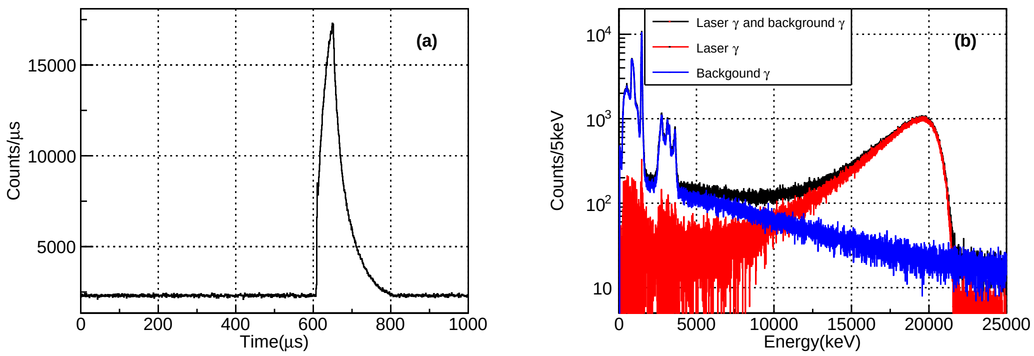

Fig. 1. (Color online) (a) The time distribution of laser gamma and background gamma within a cycle.(b) Energy spectrum distribution of laser gamma and background gamma measured using $LaBr_3$.

$LaBr_3$ detector,which was used for gamma spectrum [49–52]. The response of single energy gamma rays in the $LaBr_3$ detector was simulated using Geant4 software [53] and compared with calibration data. They showed good agreement in detection efficiency and energy deposition spectrum distribution. By simulating the response function of single energy gamma rays in $LaBr_3$ detector, the response matrix of $LaBr_3$ detector to gamma rays can be obtained. Using the response matrix, we develop a software for inverse solving laser gamma spectroscopy based on Bayesian theory [54].

The black line in Fig. 2 (a) represents the gamma spectrum of $LaBr_3$ measured at a laser angle of 145°,while the blue line represents the result of the inverse solved gamma spectrum folded the response matrix. Their good agreement indicates that the inverse solved gamma spectrum is reliable. The result of the inverse solved gamma spectrum obtained using the software is shown in Fig. 2 (b) , and its FWHM is 4.6%.

B. Collimaters and Attenuator

The coarse collimator is located 18 m away from the laser electron collision point and has ten different sizes of apertures, namely 0-5 mm, 8 mm, 10 mm, 20 mm and 30 mm. The fine collimator is 36 m away from the collision point, and its aperture can be continuously changed between 0 and 40 mm [39]. The attenuator is composed of 8 copper blocks with different thicknesses (1×200 mm, 3×100 mm, 2×50 mm, 1×25 mm and 1×15 mm) and diameters of 50 mm. The coarse collimator and fine collimator jointly adjust the energy bandwidth and beam spot size of the gamma beam, while the attenuator adjusts the beam flux to meet the requirements of nuclear physics, irradiation experiments and detector calibration.

C. Experimental station

There are three types of detectors in the experimental station, namely gamma detectors, neutron detectors, and charged particle detectors. The gamma detector consists of two HPGe detectors with a diameter of 80 mm and a thickness of 90 mm, two CLOVER detectors composed of four crystals with a diameter of 50mm and a thickness of 70 mm [40], eight $LaBr_3$ detectors with a diameter of 76.2 mm and a thickness of 101.6 mm, and one BGO detector with a diameter of 76.2 mm and a thickness of 200 mm as the beam monitor detector. The energy spectrum and flux of the beam are mainly measured using BGO and $LaBr_3$ detectors. There are 20 EJ-301 fast neutron detectors with a diameter of 127 mm and a thickness of 50.8 mm, 6 ^{3}He tubes with a diameter of 25.4 mm and a effective length of 500 mm, and 20 ^{3}He tubes with a diameter of 50.8 mm and a effective length of 500 mm. The pressure value of all ^{3}He tubes is 2 atmospheres. Charged particle detectors include six Frisch-grated ionization chambers (FGIC) with a height of 72 mm and a thickness of 64 mm, four 65 μm and two 100 μm thick single-sided silicon microstrip detectors, four 300 μm and two 500 μm double-sided silicon microstrip detectors, and six sets of sensitive area 64 mm × 64 mm cesium iodide array with a thickness of 20 mm. These charged particle detectors are combined to form a charged particle telescope system for identifying light charged particles such as p, d, t, ^{3}He and α.

The experimental station has a vacuum chamber with a diameter of 1000 mm and a height of 800 mm. Its static vacuum can reach 10^{-6} millibars and its leakage rate is less than 1×10^{-11} Pa·m^3/s.

D. Electronics and Data-acquisition system

The data acquisition system of SLEGS experimental station mainly consists of two types: one is the CoMPASS waveform digital data acquisition system [41], and the other is the MVME of Mesytec waveform digital data acquisition system [42]. According to different detector signals, each type of acquisition system has two different acquisition modes. The CoMPASS data acquisition system has Pulse Shape Discrimination (PSD) mode and Pulse Height Analysis (PHA) mode, while the MVME of Mesytec data acquisition system has Charge to Digital Converter (QDC) mode and Standard

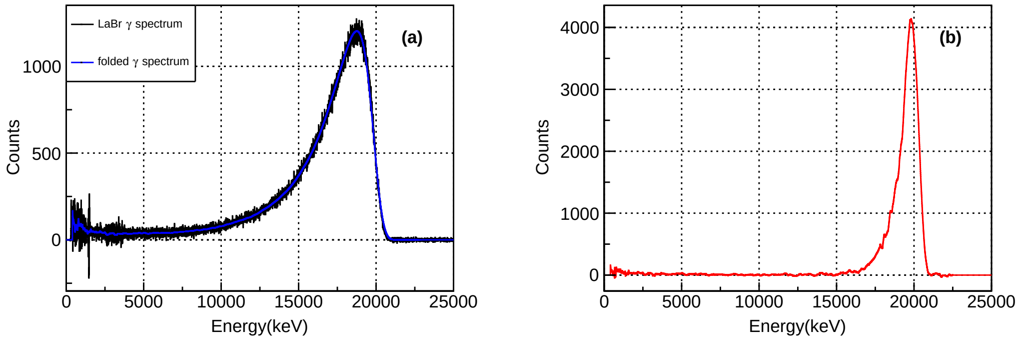

Fig. 2. (Color online) (a) Comparison between folded spectrum and experimental $LaBr_3$ spectrum at a laser angle of 145°. (b) The inverse solved gamma spectrum distribution at 145°.

Charge sensitive Preamplifier (SCP) mode. The PSD and QDC modes correspond to several hundred nanosecond pulse signals output by photomultiplier tubes and the PHA and SCP modes correspond to several to tens of microseconds of signals output by pre-amplifiers or others. The CoMPASS data acquisition system consists of 6 V1725s digitizers with a sampling frequency of 250MHz and 8 V1730s digitizers with a sampling frequency of 500MHz. The Mesytec data acquisition system consists of 4 MDPP-16 digitizers and 1 MDPP-32 digitizer.

The acquisition control interface of the data acquisition system CoMPASS mainly consists of five parts. The first part is the Run ID, where the user can set the name of the saved file and choose whether to automatically add the file's serial number. The second part is acquisition settings, which is to set the acquisition mode. There are two options: list only and wave mode, namely not saving waveform and saving waveform mode. The acquisition time can be set, and the configuration file can be selected. The third part is board buffers saving, which allows the user to choose whether to save the data of the board, mainly for offline data processing. The fourth part is data saving settings (List Saving). The user can choose to save raw data, unfiltered data, or filtered data. The format for saving data is generally ROOT, and the user can choose to limit the file size. The user can choose one file for one channel or one file for all channels, and choose whether to sort events. The energy format can choose ADC or scale values or both. The fifth part is spectra saving settings. The user can choose to save the spectrum at the end of the acquisition, or save the spectrum for a certain period of time, or not save the spectrum. The user can choose the data format for saving the spectrum, and choose to save one or more of the four spectra of Energy, PSD, Time distribution and ΔT.

The main parameters set in this acquisition system CoMPASS include polarity, discrimination mode, QDC Gate, Short Gate, and Pregate in PSD mode, rise time, flat top and pole zero in PHA mode. The EJ-301 neutron detector can achieve a time resolution of 230 ps using CFD discrimination, while the $LaBr_3$ detector can achieve a time resolution of 690 ps.

The control interface of the data acquisition system Mesytec mainly consists of four parts. The first part is the data acquisition control interface, whose main functions are to start or stop data acquisition, set the connection mode with data acquisition electronics, select whether to record data, set the time for data acquisition, set the name of the file for data recording, and select whether the file for recording data is divided by time period or file size. The second part is the VME electronics parameter configuration interface, whose main function is to set the waveform digitizers used for acquisition, set their addresses to be consistent with the hardware settings, set the firmware mode to be consistent with the hardware settings, and set the integration and differential time for signal time filtering, shaping time, rise time, decay time, etc. The third part is the data analysis interface, whose main function is to select the data source to be analyzed, perform necessary logical operations, and generate visualized one-dimensional or two-dimensional histograms. The fourth part is the Log interface, which mainly outputs information during data acquisition operations, such as the time when acquisition started and the configured electronic parameters, the time when acquisition stopped, etc. If an error occurs during the configuration process or during the acquisition process, it will be displayed in red text on this interface, and the reason for the error can be found from this information.

III. EXPERIMENTAL SPECTROMETERS

The detailed knowledge of photonuclear reaction data is great significance for various applications, such as astrophysical applications, medical-isotope production and radiation-shielding design, nuclear-waste transmutation, safeguards and inspection technologies, physics and technology of fission reactors (the influence of photonuclear reactions on the neutron balance) and fusion reactors (plasma diagnostics and shielding-activation calculations), analyses of absorbed dose in the human body during radiotherapy and radiation-transport calculations. According to the products detected in the photonuclear experiment, the experiment can be divided into five types.

A. Nuclear Resonance Fluorescence (NRF) spectrometer

The NRF spectrometer is nuclear resonance fluorescence experiments limited below neutron threshold, which only detect gamma rays generated in the reaction. The NRF spectrometer mainly measures the energy and angular distribution of the de-excited gamma rays generated in nuclear reactions, using coincidence to determine the energy level states of nuclei. The spectrometer mainly consists of 2 HPGe detectors and 2 CLOVER detectors, with a total of 8 signals output through pre-amplifiers. Therefore, the data acquisition system of the spectrometer uses Mesytec's SCP mode. Fig. 3 is the 3D model and the picture of the nuclear resonance fluorescence spectrometer. The distance between the front surface of these detectors and the beam center can be adjusted from 10 mm to 80 mm. To facilitate the measurement of polarization experiments, the position of the detectors can be rotated along the beam axis. In addition, other gamma detectors such as $LaBr_3$ can also be added to the NRF spectrometer to improve detection efficiency [43].

Nuclear resonance fluorescence can be applied to non-intrusively interrogate a region of space and measure the isotopic content of materials in that space to find any element heavier than helium. The prospect of NRF as a non-destructive analysis (NDA) technique in safety applications lies in its potential for directly quantifying specific isotopes in the target analysis. This technology involves irradiating materials to intense photon beams and detecting scattered photons with isotopic specific discrete energy distributions. The interrogating photons with energy between 2 and 8 MeV, are the most penetrating probe and are effective when the isotopes of interest are shielded by steel or other materials.

The research based on NRF used two detection schemes, namely scattering and transmission methods. In both methods, interrogation photons are used to induce resonance absorption, while de-excited photons are detected directly in the backward scattering position or indirectly in the forward self absorption position. The investigated object is placed in the beam, and resonant photons are detected in the backward scattering position by detectors located off-beam in scattering experiments.

It is worth mentioning that NRF-NDA technology can be used for various other applications that require isotope identification. For instance, some suggest applying this technology to cultural heritage research. The penetrability of γ will make it possible to study bulk objects, complex archaeological artifacts, and artworks. With the increase of beam intensity, these NDA methods will be further developed.

B. Flat-Efficiency Neutron Detector (FED) spectrometer

The FED spectrometer is used for the experiments that exceed the neutron threshold, which only detect the neutrons produced in the reaction. The FED spectrometer mainly consists of 26 ^{3}He neutron tube detectors embedded in a 450 mm $\times$ 450 mm $\times$ 550 mm polyethylene moderator. There is a layer of 2 mm cadmium and a layer of 50 mm polyethylene on the outer surface of the moderator. The neutron tubes are divided into three rings, with radii of 65 mm, 110 mm, and 175 mm for each ring. The first ring has 6 neutron tubes with a diameter of 25.4 mm. The second and third rings have 8 and 12 neutron tubes with a diameter of 50.8 mm, respectively. The signal of the neutron tube is output by the pre-amplifier, so the data acquisition system of the spectrometer uses the SCP mode of the Mesytec acquisition system. Fig. 4 is the 3D model and the picture of the flat efficiency neutron spectrometer. Its detection efficiency with californium source calibration is 42.1%. This spectrometer is mainly used for measuring the photoneutron cross-section, but it cannot accurately determine the energy of neutrons [44].

Photonneutron cross-section measurement is based on the slow down, i.e., thermalization of neutrons, which are then converted into charged particles using a neutron detector. The neutron multiplicity of moderated neutrons is measured in the experiment. There are two different techniques used to estimate the number of measured neutrons, namely flatness efficiency [45] and ring-ratio techniques [46]. This spectrometer adopts a combination of flat efficiency and ring-ratio technology.

The outermost ring is relatively more sensitive to high-energy neutrons than the innermost ring because there is more moderate material between the outermost detector and the target. Therefore, the ratio of the number of neutrons detected in the outermost ring to the number of neutrons detected in the innermost ring, known as the ring ratio, varies with the variation of the average neutron energy. The goal of flat efficiency technology is to directly measure neutron multiplicity. The main design idea is to place the neutron counter in a moderator in such a way that for energy up to 7 MeV, the detection efficiency does not depend on the neutron kinetic energy. Not only does it require a flat efficiency over a wide energy range, but it also requires high detection efficiency for reactive neutrons.

It is impossible to achieve a constant detection efficiency of the FED spectrometer with the energy of neutrons. Therefore, we first use the ring ratio method to determine the energy of neutrons, and then determine the detection efficiency of the FED spectrometer based on the variation of detection efficiency with the energy of neutrons. Based on the detection efficiency of the FED spectrometer, the multiplicity of neutrons is ultimately determined.

C. Neutron time-of-flight (TOF) spectrometer

The experiment of the neutron time of flight spectrometer is similar to the second one, but requires neutron gamma coincidence measurements. Fig. 5 (a) is the structural design diagram of the neutron time of flight spectrometer, and its photo is shown in (b). The lanthanum bromide gamma detector is located below the target in the opposite direction of the beam, 30 cm away from the target. The EJ301 fast neutron detector is located above the target in the opposite direction of the beam, at a distance of 150 cm from the target. The gamma detector provides the start time of the event, while the

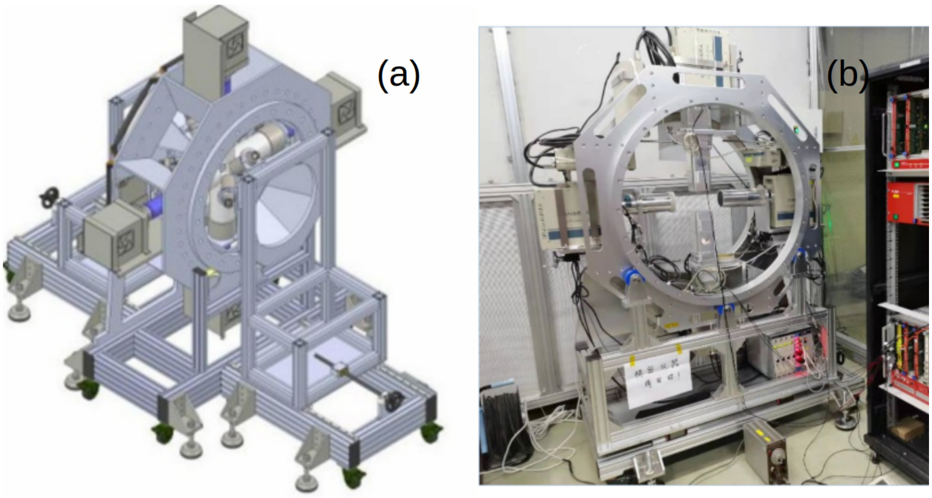

Fig. 3. (Color online) (a) 3D model of the nuclear resonance fluorescence spectrometer.(b)The nuclear resonance fluorescence spectrometer.

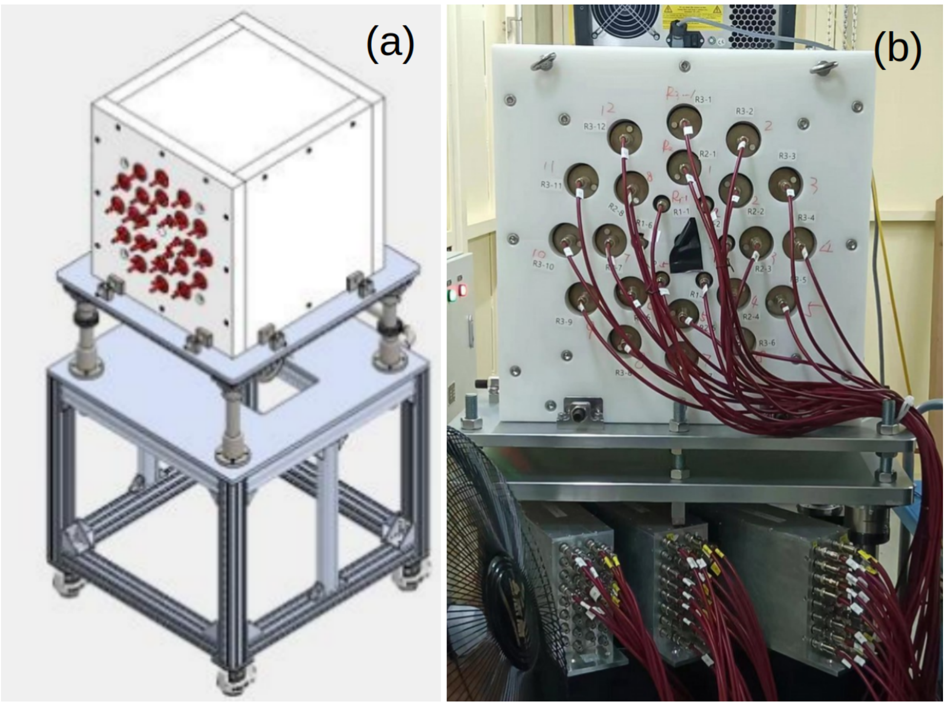

Fig. 4. (Color online) (a) 3D model of the Flat-Efficiency Neutron Detector spectrometer.(b)The Flat-Efficiency Neutron Detector spectrometer.

neutron detector provides the end time of the event, thus obtaining the flight time of the neutron. The energy of neutrons produced in photoneutron reactions can be obtained from the flight time of neutrons. The neutron time of flight spectrometer mainly consists of 8 $LaBr_3$ detectors and 20 EJ301 neutron detectors, with a total of 28 signals. These signals are short pulse signals output by photomultiplier tubes. Therefore, the data acquisition system of the neutron time of flight spectrometer utilizes the PSD mode of the CoMPASS data acquisition system. The data acquisition system uses the A3818 and V2718 fiber optic bridge mode to connect the data acquisition hardware with computer software. Two V1730S waveform digitizers with a sampling frequency of 500MHz are selected to collect the detector signal and perform analog-to-digital conversion. Two digitizers need to synchronize their clocks to achieve neutron gamma coincidence measurement. This spectrometer can achieve a time resolved half maximum width of 1 ns to 1.5 ns. Therefore, high neutron energy accuracy measurement can be achieved.

This spectrometer can determine the partial energy level states of certain nuclei in photonuclear reactions. The types, granularity, and positions of neutron and gamma detectors in

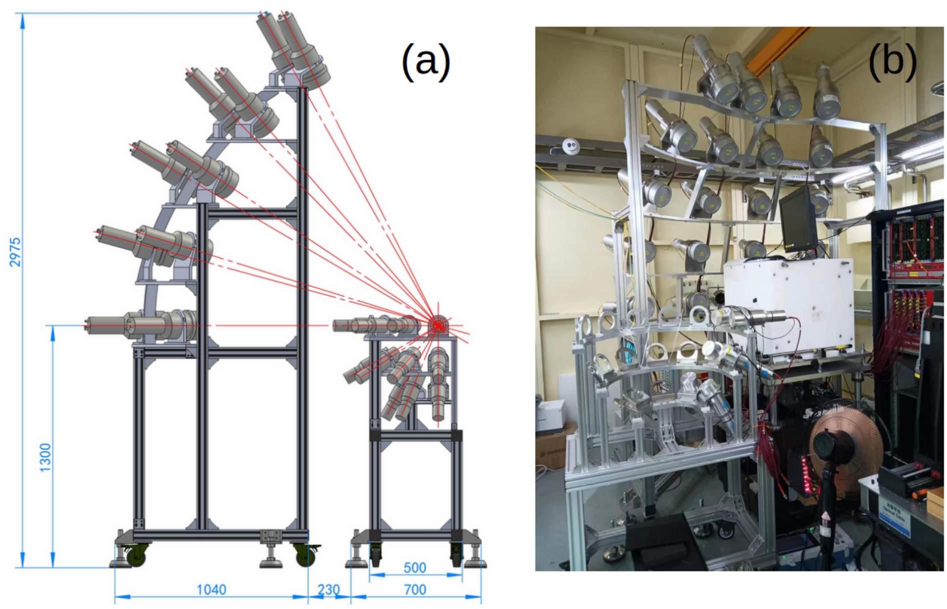

Fig. 5. (Color online) (a) Structural design diagram of the neutron time-of-flight spectrometer.(b)The neutron time-of-flight spectrometer.

the spectrometer can be redesigned according to experimental needs, such as polarization experiments [47]. To measure the angular distribution of neutrons, the angle of the γ photons's linearly polarized plane is tuned by changing the polarization plane of incident laser.

D. Light charged particle (LCP) spectrometer

The light charged particle spectrometer is used for the experiments that exceed the threshold of proton or other light charged particle, mainly detecting various light charged particles. Fig. 6 (a) and (b) show the 3D model of the light charged particle spectrometer and the on-site test photo, respectively. Fig. 6 (c) is the layout diagram of the design scheme for the light charged particle spectrometer. Gamma beam incident in the positive direction along the Y-axis. The entire spectrometer is placed in a vacuum target chamber. The spectrometer in the figure consists of four particle telescope systems, which are placed at different angles on both sides of the beam, at a distance of 25 cm from the target. Each particle telescope system consists of a frisch-grated ionization chamber, a silicon microstrip detector, and a nine unit cesium iodide detector array. Each telescope is an $\Delta E - \Delta E - E$ light charged particle identification system that can identify particles such as proton, deuterium, tritium, ^{3}He, and α. The spectrometer is mainly used for nuclear physics experiments studying the structure of nuclei clusters [48].

E. Photon activation analysis spectrometer

The photon activation analysis spectrometer is designed for offline measurement of gamma activation experiments, measuring the gamma generated by product decay. The study of medical isotopes requires the method of photon activation analysis. The experimental station has designed and constructed a photon activation analysis spectrometer consisting of a HPGe detector with a diameter of 67mm and a length of 65mm. The background counting rate of the spectrometer can reach 5 counts per second. Fig. 7 shows the background spectrum measured by the HPGe detector in a shielded cavity.

The research of SLEGS in the field of medical radioactive isotopes will focus on evaluation of the specific activity yields for medical radioactive isotopes produced in different photonuclear reactions and detailed cross-section calculations. Design experimental research to search for new production routes for medical radioactive isotopes, such as measurement of the specific activity of medical radioactive isotopes produced in photonuclear reactions, and measuring the production of medical radioactive isotopes of interest (γ, p) and (γ, n) cross section of the reaction and finding the doorway state for population of isomer in medical radioactive isotopes of interest.

IV. TEST EXPERIMENTAL RESULTS OF SLEGS

The photoneutron reaction cross-sections of targets such as ^{197}Au and ^{159}Tb have been measured using the flat efficiency neutron detector spectrometer and preliminary data processing has been carried out. The measurement results are in good agreement with those of other international laboratories. The (γ,n) reaction of ^{nau}Pb target was tested using a neutron time of flight spectrometer. Twenty EJ301 neutron detectors were used in the experiment, with a distance of 150 cm from the target. Six $LaBr_3$ detectors were used, with a distance of 30 cm from the target. The neutron time-of-flight

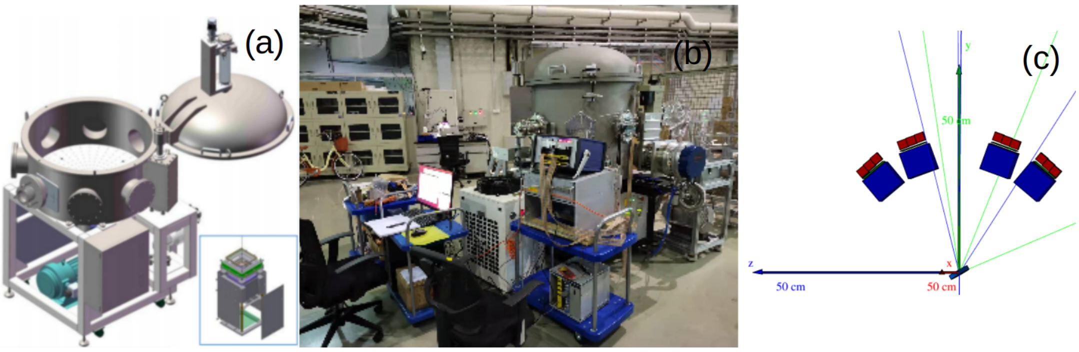

Fig. 6. (Color online) (a) 3D model of the light charged particle spectrometer.(b) The photo of the light charged particle spectrometer testing site. (c)Schematic drawing of the light charged particle spectrometer.The blue block represents the screen ionization chamber, the green thin layer represents the Si detector, and the red block represents the CsI detector.

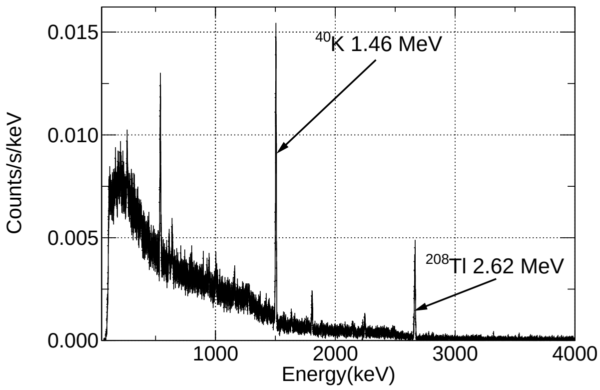

Fig. 7. The Background Spectra of HPGe Measurement.

spectrum measured in the experiment ranges from 40 to 200 ns. The peaks of 569.6 keV, 897.3 keV of product ^{207}Pb, and 803.1 keV of product ^{206}Pb were clearly distinguished in the gamma spectrum. The gamma flux measured at various laser incidence angles using the photon activation analysis spectrometer is consistent with the flux measured using the $LaBr_3$ detector. Experiments on the NRF spectrometer and the LCP spectrometer are also ongoing and planned.

V. CONCLUSION

The SLEGS beamline at SSRF is a powerful platform to investigate the GDR, PDR and MDR for research in field of the s-process and p-process nucleosynthesis, nuclear transmutation and so on. At present, photon-induced nuclear reaction data can be collected in neutron FED spectrometer and neutron TOF spectrometer methods. In addition, gamma NRF spectrometer and LCP spectrometer methods will be grandually available to users in the future.

ACKNOWLEDGEMENTS

We acknowledge to the beamline engineers from SSRF Optics and Control Department, Mechanic and Vacuum Department, thanks for their hard works on beamline design, construction and online testing. We are very grateful to Zhao Zhentang, Tai Renzhong, Wang Jie, Huang Yuying, and Xue Song, all of them have discussed deeply with us on detector techniques and the beamline design. Thanks to Researcher Zhang Guilin, for his assistance in testing detectors. Thanks to Researcher Jin Genming from the Institute of Modern Physics, for his guidance on the experimental methods. We would like to thanks Professor Wen Wanxin from Suzhou University for developing a gamma beam spot measurement device for us. We appreciate the support of Guo Bing, He Chuangye, Liu Fulong, Wang Zhiqiang, Liu Yina, and Song Mingzhe from the Chinese Academy of Atomic Energy Sciences in the calibration of $LaBr_3$ detectors. We would like to express our gratitude to Professor Hiroaki Utsunomiya for his guidance in gamma spectroscopy measurement. The authors are grateful to Academicians Shen Wenqing and Ma Yugang for their guidance in the construction of the SLEGS beamline. This work is supported by the Shanghai Light Source Line Station Project.

[1] A. Zilges, D.L. Balabanski, J. Isaak, N. Pietralla, Photonuclear reactions—From basic research to applications,Progress in Particle and Nuclear Physics,**122**,103903,(2022). doi:10.1016/j.ppnp.2021.103903

[2] S. Lindenstruth, A. Degener, R.D. Heil et al., Measurements and simulations of low energy, thick target bremsstrahlung spectra, Nuclear Instruments and Methods in Physics Research Section A,**300**,(2)293-296,(1991). doi:10.1016/0168-9002(91)90439-W

[3] R. Schwengner, R. Beyer, F. Dönau et al., The photon-scattering facility at the superconducting electron accelerator ELBE,Nuclear Instruments and Methods in Physics Research Section A,**555**,(1) 211-219,(2005). doi:10.1016/j.nima.2005.09.024

[4] K. Kosako,K. Oishi, T. Nakamura et al., Angular Distribution of Bremsstrahlung from Copper and Tungsten Targets Bombarded by 18, 28, and 38MeV Electrons,Journal of Nuclear Science and Technology,**47**,(3) 286-294,(2010). doi:10.1080/18811248.2010.9711956

[5] P. Mohr, J. Enders,T. Hartmann et al.,Real photon scattering up to 10MeV: the improved facility at the Darmstadt electron accelerator S-DALINAC ,Nuclear Instruments and Methods in Physics Research Section A,**423**,(2) 480-488,(1999). doi:10.1016/S0168-9002(98)01348-5

[6] Flerov Laboratory of Nuclear Reactions, 2024, http://flerovlab.jinr.ru/mt-25-microtron/ Accessed: 2024-01-28.

[7] Accelerating new discoveries in nuclear physics, 2024, https://www.llnl.gov/article/45861/accelerating-new-discoveries-nuclear-physics Accessed: 2024-01-28.

[8] W. Bertozzi,J.A. Caggiano,W.K. Hensley et al., Nuclear resonance fluorescence excitations near 2 MeV in ^{235}U and ^{239}Pu.Phys. Rev. C **78**(4)041601 (2008). doi:10.1103/PhysRevC.78.041601

[9] National Science Center Kharkov Institute of Physics and Technology, 2024, https://www.kipt.kharkov.ua/en/ Accessed: 2024-01-28.

[10] The Idaho Accelerator Center, 2024, https://www.isu.edu/physics/facilities–research/idaho-accelerator-center- iac/ Accessed: 2024-01-28.

[11] D. Savran, K. Lindenberg, J. Glorius et al.,The low-energy photon tagger NEPTUN,Nuclear Instruments and Methods in Physics Research Section A,**62**,(1) 257-303,(2009). doi:10.1016/j.ppnp.2008.07.001

[12] H.R. Weller, M.W. Ahmed,H. Gao et al.,Research opportunities at the upgraded HIγS facility,Progress in Particle and Nuclear Physics,**613**,(2) 232-239,(2010). doi:10.1016/j.nima.2009.11.038

[13] H.R. Weller, M.W. Ahmed,Y. K. Wu ,Nuclear Physics Research at the High Intensity Gamma-Ray Source (HIγS),Nuclear Physics News,**25**,19-24,(2015). https://api.semanticscholar.org/CorpusID:120009084

[14] H. Zen,H. Ohgaki,Y. Taira et al.,Demonstration of tomographic imaging of isotope distribution by nuclear resonance fluorescence,AIP Advances,**9**,(3) 035101,(2019). doi:10.1063/1.5064866

[15] D. Angal-Kalinin, G. Arduini, B. Auchmann et al.,PERLE. Powerful energy recovery linac for experiments. Conceptual design report,Journal of Physics G: Nuclear and Particle Physics,**45**,(6) 065003,(2018). doi:10.1088/1361-6471/aaa171

[16] M.W. Krasny, The Gamma factory proposal for CERN,2015.

[17] C. Curatolo, W. Placzek, M.W. Krasny, L. Serafini, M. Zanetti, PoS LHCP2018 (2018) 089.

[18] M.W. Krasny, A. Petrenko, W. Płaczek, High-luminosity Large Hadron Collider with laser-cooled isoscalar ion beams,Progress in Particle and Nuclear Physics,**114**, 103792,(2020). doi:10.1016/j.ppnp.2020.103792

[19] D. Budker, J.R. Crespo López-Urrutia, A. Derevianko et al., Atomic Physics Studies at the Gamma Factory at CERN,Ann. Physics,**532**, 2000204,(2020). doi:10.1002/andp.202000204

[20] X.Z. Cai, J.H. Gu, W. Guo et al., Research on properties and application of Compton backscattered gamma light source based on synchrotron radiation accelerator. Prog. Phys. **23**, 389 (2003). doi:10.3321/j.issn:1000-0542.2003.04.001(in Chinese)

[21] W. Guo, W. Xu, J.G. Chen et al., A high intensity beam line of γ-rays up to 22 MeV energy based on Compton backscattering. Nucl. Instr. Meth. A **578**, 457 (2007). doi:10.1016/j.nima.2007.05.32214

[22] J.G. Chen, W. Xu, W. Guo et al., An X-ray source based on Compton backscattering of CO2 laser and 100 MeV electrons. Nucl. Instr. Meth. A **580**, 1184–1190 (2007). doi:10.1016/j.nima.2007.07.00715

[23] W. Luo, W. Xu, Q.Y. Pan et al., Laser Compton scattering experiments and the latest developments in construction of experimental facilities at SINAP. SPIE **7385**, 73852D(2009) doi:10.1117/12.83557216

[24] W. Luo, W. Xu, Q.Y. Pan et al., A laser-Compton scattering(LCS) prototype experiment at 100MeV Linac of Shanghai Institute of Applied Physics. Rev. Sci. Instr. **81**, 013304 (2010). doi:10.1063/1.328244517

[25] W. Luo, W. Xu, Q.Y. Pan et al., An X-ray spectroscopy system and its application to the Laser-Compton scattering experiments. Nucl. Instr. Meth. A **624**, 141–147 (2010). doi:10.1016/j.nima.2010.09.04518

[26] W. Luo, W. Xu, Q.Y. Pan et al., A 4D Monte Carlo laser-Compton scattering simulation code for the characterization of the future energy-tunable SLEGSA 4D Monte Carlo laser-Compton scattering simulation code for the characterization of the future energy-tunable SLEGS. Nucl. Instr. Meth. A **660**, 108–115 (2011). doi:10.1016/j.nima.2011.09.03519

[27] W. Luo, W. Xu, Q.Y. Pan et al., X-ray generation from slanting laser-Compton scattering for future energy-tunable Shanghai Laser Electron Gamma Source. Appl. Phys. B **101**, 761–771(2010). doi:10.1007/s00340-010-4100-020

[28] H. XU, Z. ZHAO, Current status and progresses of SSRF project. Nuclear Science and Techniques **19**, (1) (2008). doi:10.1016/S1001-8042(08)60013-5

[29] G. Baldwin, G. Klaiber, Phys.Rev. **71** (3).

[30] O. Wieland, A. Bracco, F. Camera et al., Giant dipole resonance in the hot and thermalized ^{132}Ce nucleus: Damping of collective modes at finite temperature. Phys. Rev. Lett. **97** (2006). doi:10.1103/2

[31] A.Shiller, M.Thoennessen,Atomic Data and Nuclear Data Tables **93** (549).

[32] H.W. Wang, G.T. Fan, L.X. Liu et al., Development and prospect of shanghai laser Compton scattering gamma source. Nucl. Phys. Rev. **37**(1), 53–63 (2020). doi:10.11804/NuclPhysRev.37.2019043 (in Chinese)

[33] N. Paar, D. Vretenar, E. Khan et al., Exotic modes of excitation in atomic nuclei far from stability. Reports on Progress in Physics **70** (5) (2007). doi: 10.1088/0034-4885/70/5/R02

[34] A. Carbone, G. Colò, A. Bracco et al., Constraints on the symmetry energy and neutron skins from pygmy resonances in ^{68}Ni and ^{132}Sn. Phys. Rev. C **81**, 041301 (2010). doi:10.1103/PhysRevC.81.041301

[35] H. Utsunomiya, S. Goriely, H. Akimune et al., Photoneutron cross sections for ^{96}Zr: A systematic experimental study of photoneutron and radiative neutron capture cross sections for zirconium isotopes. Phys. Rev. C **81**, 014615 (2010). doi:10.1103/PhysRevC.81.035801

[36] V. Kaur, S. Kumar, Systematic study of multifragmentation in asymmetric colliding nuclei. Phys. Rev. C **81**, 064610 (2010). doi:10.1103/PhysRevC.81.064610

[37] H.W. Wang, G.T. Fan, L.X. Liu et al., Commissioning of laser electron gamma beamline SLEGS at SSRF. Nuclear Science

and Techniques **33**, 2210–3147 (2022). doi:10.1007/s41365-022-01076-0

[38] H. Xu, G. Fan, H. Wang et al., Interaction chamber for laser compton slant-scattering in SLEGS beamline at shanghai light source. Nucl. Instr. Meth. A **1033**, 166742 (2022). doi:10.1016/j.nima.2022.166742

[39] Z. Hao, G. Fan, H. Wang et al., Collimator system of slegs beamline at shanghai light source. Nucl. Instr. Meth. A **1013**, 165638 (2021). doi:10.1016/j.nima.2021.165638

[40] G. Duchêne, F. Beck, P. Twin et al., The clover: a new generation of composite Ge detectors. Nucl. Instr. Meth. A **432**, (1) (1999) 90–110. doi:10.1016/S0168-9002(99)00277-6

[41] CAEN:https://www.caen.it [online].2023.

[42] Mesytec. https://www.mesytec.com [online]. 2023.

[43] P. Kuang, L.L. Song, K.J. Chen et al., Design and detector performance analysis of Shanghai Laser Electron Gamma Source (SLEGS) nuclear resonance fluorescence spectrometer.Nucl. Phys. Rev. **40**,(1):58-65 (2023). doi:10.11804/NuclPhysRev.40.2022040(in Chinese)

[44] Z.R. Hao, G.T. Fan, L.X. Liu et al., Design and simulation of 4π flat-efficiency 3He neutron detector array. NUCLEAR TECHNIQUES **43**, (11):110501 (2020). doi:10.11889/j.0253-3219.2020.hjs.43.110501

[45] L.V. East, R.B. Walton, Polyethylene moderated 3He neutron detectors. Nuclear Instruments and Methods **72**, (2) 161-166 (1969). doi:10.1016/0029-554X(69)90152-9

[46] B.L. Berman, J.T. Caldwell,R.R. Harvey et al., Photoneutron Cross Sections for Zr^{90}, Zr^{91}, Zr^{92}, Zr^{94}, and Y^{89}. Phys. Rev. **162**, (4) 1098–1111 (1967). doi:10.1103/PhysRev.162.1098

[47] K.J. Chen, L.X. Liu, Z.R. Hao et al., Simulation and test of the SLEGS TOF spectrometer at SSRF. NUCL SCI TECH **34**, 47 (2023). doi:10.1007/s41365-023-01194-3

[48] T.L. Qiu, M. Li, X.L. Wei et al., Ion pulse ionization chamber for online measurements of the radon activity concentration. NUCLEAR TECHNIQUES **44**,(4):040403 (2021). doi:10.11889/j.0253-3219.2021.hjs.44.040403

[49] F.L. Liu, C.Y. He, H.R. Wang et al., Thick-target yield of 17.6MeV γ ray from the resonant reaction ^{7}Li(p,γ)^{8}Be at E_p =441keV. Nucl. Instr. Meth. B **529**, 56-60 (2022). doi:10.1016/j.nimb.2022.08.005

[50] A. Antilla, J. Keinonen, M. Hautala, I. Forsblom, Use of the ^{27}Al(p,γ)^{28}Si, E_p = 992 keV resonance as a gamma-ray intensity standard. Nucl. Instr. Meth. **147** (1977) 501-505. doi:10.1016/0029-554X(77)90393-7

[51] Y.L. Dang, F.L. Liu, G.Y. Fu et al., New measurement of thick target yield for narrow resonance at E_x=9.17MeV in the ^{13}C(p,γ)^{14}N reaction. Chinese Phys. B **28**, 060706 (2019). doi:10.1088/1674-1056/28/6/060706

[52] F.L. Liu, W.S. Yang, J.H. Wei et al.Study on γ-ray source from the resonant reaction ^{19}F(p,$\alpha\gamma$)^{16}O at E_p= 340 keV. Chinese Phys. B **29**, 070702 (2020). doi:10.1088/1674-1056/ab96a0

[53] S. Agostinelli, J. Allison, K. Amako et al., Geant4—a simulation toolkit. Nucl. Instr. Meth. A **506** (3) (2003) 250–303. doi:10.1016/S0168-9002(03)01368-8

[54] G. D'Agostini, A multidimensional unfolding method based on bayes' theorem. Nucl. Instr. Meth. A **362** (2) (1995) 487–498. doi:10.1016/0168-9002(95)00274-X